

The NSTX fast-ion D-alpha diagnostic^{a)}

M. Podestà,¹ W. W. Heidbrink,¹ R. E. Bell,² and R. Feder²

¹Department of Physics and Astronomy, University of California Irvine, California 92697, USA

²Princeton Plasma Physics Laboratory, Princeton, New Jersey 08543, USA

(Presented 12 May 2008; received 10 May 2008; accepted 9 June 2008; published online 31 October 2008)

A new diagnostic, aimed at energy-resolved measurements of the spatial and temporal dynamics of fast ions in NSTX plasmas, is described. It is based on active charge-exchange recombination spectroscopy. The fast-ion signal is inferred from light emitted in the wavelength range of the D_α line by fast ions recombining with an injected neutral beam. Two complementary systems are operational. The first system, based on a spectrometer coupled to a charge coupled device detector, has 16 channels with space, time, and energy resolution of 5 cm, 10 ms, and 10 keV, respectively. The second system monitors the energy-integrated fast-ion signal on time scales of $\sim 20 \mu\text{s}$ at three different radii. Signals are measured by a multianode photomultiplier tube. For both systems, each channel includes two paired views, intercepting and missing the neutral beam for a direct subtraction of the background signal not associated with fast ions. Examples of signals from the 2008 NSTX run are presented. © 2008 American Institute of Physics. [DOI: 10.1063/1.2956744]

I. INTRODUCTION

Fast ions inside a plasma volume illuminated by a neutral beam (NB) can undergo charge-exchange reactions. A fraction of recombining fast ions is eventually excited by plasma collisions and undergoes a $3 \rightarrow 2$ transition. The emitted photon has an energy corresponding to the D_α (or Balmer-alpha) wavelength range. Due to their higher energy with respect to the thermal (or *bulk*) ions, light from recombining fast ions appear in the blueshifted and redshifted tails of the D_α spectrum.¹ The fast-ion D-alpha (FIDA) diagnostic is aimed at measuring the tails of the D_α spectrum, producing signals $s(\lambda)$ given by

$$s = s_f + B, \quad (1)$$

where B is the background light not associated with fast ions, e.g., from cold D_α , bremsstrahlung, and impurities, and s_f is the fast-ion signal,²

$$s_f(\lambda) \equiv \iint W F_f dE dp. \quad (2)$$

$F_f(E, p)$ is the local fast-ion distribution function. E and $p = v_{f,\parallel} / v_f$ are the energy and pitch parameters (v_f is the fast-ion velocity and $v_{f,\parallel}$ its component along the magnetic field). The response function, $W(E, p | \lambda)$, accounts for the effective averaging over the phase space intrinsic to the method² and for the specific viewing and beam geometry. It also contains the information on the recombination rate of fast ions, i.e., $W \propto F_b \langle \sigma_{cx} | \mathbf{v} | \rangle$, where F_b is the local distribution of injected neutrals, \mathbf{v} the relative (impact) velocity, and σ_{cx} the charge-exchange cross section. The wavelength λ depends on the energy of the emitted photons through the Doppler-shift for-

mula $\lambda = \lambda_0 (1 \pm v_f' / c)$, where λ_0 is the wavelength of the unshifted cold D_α line and c is the speed of light. v_f' is the projection of the recombining fast-ion velocity along the FIDA line of sight, responsible for the observed Doppler shift. From Eq. (2), the measured signal represents a one-dimensional sampling of $F_f(E, p)$ at that location, convolved with the response function, W . Unfolding the original form of F_f would require the inversion of Eq. (2) based on measurements from multiple lines of sight.³ On NSTX, a single sightline is available for each radial position. Two approaches are possible to interpret the experimental data. First, the data are compared with the output of a FIDA simulation code for a known F_f , calculated, for example, by the TRANSP code.⁴ This allows one to check (i) the consistency of the measurements for known plasma conditions and (ii) the validity of specific physical models adopted in TRANSP, e.g., to mimic anomalous fast-ion transport of fast-ion acceleration by radio-frequency waves.² (More details on the FIDA code are given in Refs. 1 and 2.) Second, the integrated fast-ion signal is approximated as

$$\int_{\Delta\lambda} s_f d\lambda \propto n_f n_b \langle \sigma_{cx} \bar{v} \rangle \quad (3)$$

from which the FIDA density n_f can be readily obtained from the experimental data. The integral of the measured s_f is performed over the wavelength range, $\Delta\lambda$, corresponding to the expected fast-ion energy range. \bar{v} is an average impact velocity, and $\langle \sigma_{cx} \bar{v} \rangle$ is calculated by averaging over the known fractions of NB neutrals with different injection energies, including full, 1/2, and 1/3 energy components. This approximate expression is justified by the fact that σ_{cx} is a smooth function of \bar{v} for the energy range of interest, $E \geq 20$ keV. The term n_b represents the local beam neutral density and is calculated from a beam-attenuation code. We refer to n_f as the FIDA density to highlight that it represents

^{a)}Contributed paper, published as part of the Proceedings of the 17th Topical Conference on High-Temperature Plasma Diagnostics Albuquerque New Mexico May 2008.

a sampling of the fast-ion density through the response function, W . Therefore it is only an approximate representation of the actual fast-ion density. A detailed analysis of the errors made by using Eq. (3) instead of Eq. (2) is beyond the scope of this paper and will be the subject of future work. The main experimental complication in calculating n_f is due to the fact that $s_f \ll B$. Therefore, accurate background subtraction is required to unfold the fast-ion features, as discussed in the following.

The range of applications of FIDA for tokamak physics spans from the study of fast-ion induced losses and redistribution by Alfvén waves^{5,6} to the characterization of ion acceleration following the injection of radio-frequency waves.² The FIDA systems will naturally complement the information already available from the other NSTX fast-ion diagnostics, including neutral particle analyzers,^{7,8} neutron detectors, and a scintillator based energetic ion loss detector.⁹ This paper describes the FIDA diagnostic system installed on NSTX. The diagnostic layout is presented in Sec. I. In Sec. II, the background subtraction method based on the paired views is discussed. Examples of FIDA signals from the 2008 NSTX run are illustrated in Sec. III.

II. DIAGNOSTIC LAYOUT

As anticipated in Ref. 10 two complementary instruments have been installed on NSTX. A spectrometer (s-FIDA) measures spectra in the D_α range with good spatial and spectral resolutions, but a temporal resolution limited to 10 ms. A “filter” system (f-FIDA) integrates the D_α light over a convenient spectral range. It is aimed at high temporal resolution ($\ll 1$ ms), with limited spatial and energy resolutions. Each *channel* of the two systems consists of two paired views, spaced toroidally by 30° , intercepting and missing the NB at the same radial location [Fig. 1(a)]. The net signal results from the difference between these *active* and *passive* views. Ideally, this allows one to remove all the background signals.

Light from vertical views is collected through lenses installed at the top and at the bottom of the vacuum vessel [Fig. 1(b)] at two toroidal locations. In particular, the fibers of the s-FIDA system are installed on two top ports, and those of the f-FIDA on the bottom ports. At each port, two lenses (200 mm, $f/1.8$ and 135 mm, $f/1.8$) are used to cover the region from $R=85$ cm to $R=155$ cm on the equatorial plane (R is the coordinate along the major radius) (see Fig. 1). From the lenses, the light is focused onto optical fibers with diameters of $800 \mu\text{m}$ (inner views) and $600 \mu\text{m}$ (outer views) and length ≈ 45 m. The s- and f-FIDA systems include 2×16 and 2×3 views, respectively. The signals are then transported outside of the NSTX test cell to the FIDA systems. This limits noise and possible damages to the detectors from neutrons and γ emission.

The s-FIDA system is illustrated in Fig. 2(a). Referring to the tags in the figure, the 2×16 fibers from the active and passive views are arranged in two columns on the entrance slits (1). An input lens (2) focuses the input light into parallel rays, impinging on a dispersion grating (3).¹¹ A bandpass filter is mounted at the output of (2) to cut out wavelengths

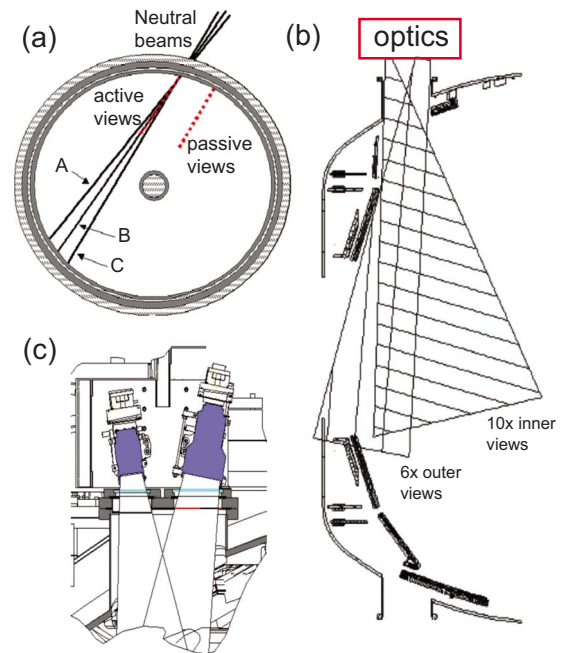


FIG. 1. (Color online) (a) Equatorial cross section of NSTX showing the paths of the three NB sources (A, B, and C) and the location of the FIDA active and passive views. (b) Poloidal cross section and field of view of the “top” lenses, used for the s-FIDA views, highlighted. The “bottom” lenses, used for the f-FIDA fibers, are symmetric with respect to the equatorial plane. (c) Details of the two lenses installed at each of the four ports occupied by the FIDA views.

outside the 645–667 nm range. After the grating, an output lens (4) refocuses the rays on the image plane (5). Here, the bright emission from cold D_α is filtered out by narrow (≤ 1 mm) strips, obtained from a neutral density filter with

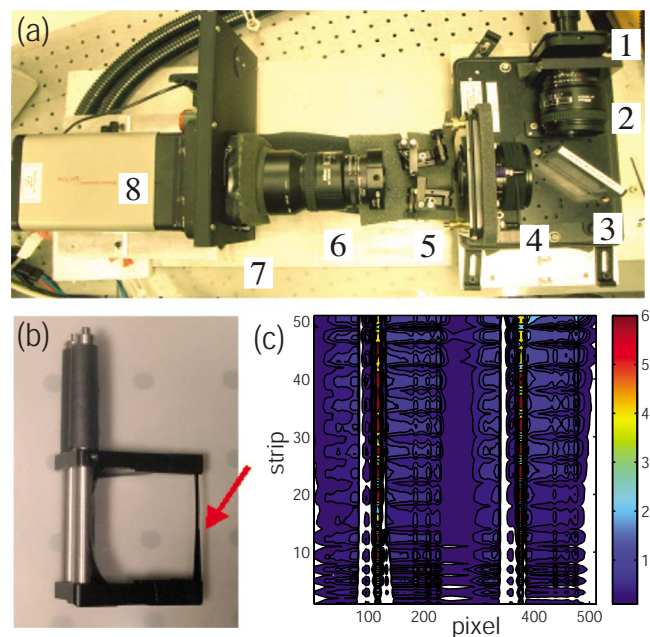


FIG. 2. (Color online) (a) Picture of the s-FIDA system. (b) Detail of the opaque strip, indicated by the arrow, used to attenuate the cold D_α emission. (c) Example of a frame collected by the CCD detector during a plasma discharge. The brightest regions correspond to the attenuated cold D_α lines. The 2×16 spectra are rebinned into 51 regions on the detector (visible as horizontal strips) to avoid saturation and to increase the dynamic range.

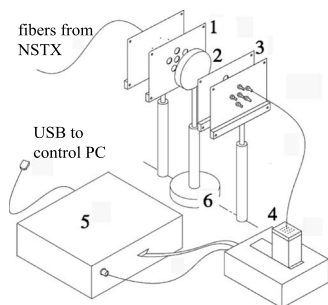


FIG. 3. Schematic of the f-FIDA system.

1% transmission [Fig. 2(b)]. By doing that, information on both the fast and cold D_α components are simultaneously available [see Fig. 5(a)], thus expanding the effective dynamic range of the instrument. Finally, the image of the 2×16 spectra is demagnified by two lenses (85 mm, $f/1.8$ and 50 mm, $f/1.2$), mounted in a back-to-back configuration (6), and acquired by a high quantum efficiency charge coupled device (CCD) camera (8) [Fig. 2(c)]. An optical chopper (7), synchronized with camera timing via a timing unit developed at PPPL, prevents light from reaching the detector during the CCD read-out phase. Except for the bandpass filter, components (1)–(5) are included in a commercial spectrometer. Most of the optical components, including the spectrometer, the camera, the demagnifying lenses, and the filter strips, are mounted on translation stages. This allows a precise alignment of the system and an accurate and independent focusing at the different focal planes. The 16 channels of the s-FIDA system cover the range $R=85$ – 155 cm, resulting in a spatial resolution of 5 cm. This is comparable with the intrinsic resolution of the method, determined by the effective lifetime of the $n=3$ excited state.⁶ The energy resolution given by the entrance slits is 10 keV for the present setup, with a temporal resolution of 10 ms. The details on the hardware parts are reported under Ref. 12.

A schematic of the f-FIDA system is shown in Fig. 3. Light from NSTX is collected by six fiber bundles, each comprising seven fibers to enhance the signal. The optical part includes input and output lenses (1–3) to focus and demagnify the beam spots. A bandpass filter (2) selects emission in the 650–655 nm range. The output signal is refocused onto six fibers (diameter 2 mm) and measured by a multianode photomultiplier tube (4). Finally, a charge-integrating acquisition system (5) transfers the data to a control PC, from which it is stored into the NSTX MDS-PLUS tree. The orientation of the filter, hence its actual bandpass range, can be adjusted through a rotation stage (6). This makes it possible to perform a rough spectral scan on a shot-to-shot basis. The three lines of sight of the f-FIDA system collect light from $R=100$, 120, and 140 cm. Depending on the specific experimental conditions, sampling rate and integration time can be remotely adjusted to optimize the signal-to-noise ratio. For standard NSTX discharges ($n_e \sim 3 \times 10^{19} \text{ m}^{-3}$, $T_e \leq 1 \text{ keV}$, and two NB sources with beam voltage =90 kV), a sampling rate of 50 kHz is used. The maximum sampling rate supported by the acquisition system

is 150 kHz. Details on the different components of f-FIDA are given in Ref. 13.

III. BACKGROUND SUBTRACTION

A major issue for the FIDA technique is represented by background subtraction [see Eq. (1)]. In previous experiments, where no background views were available, two different approaches were used.¹ For stationary discharges, an on/off modulation of the NB power was used to estimate the background from the NB off phase. When discharges were not stationary, the background was modeled and removed from the measured spectra through a software-implemented analysis. For typical NSTX discharges, however, plasma parameters such as density and temperature vary in time throughout the discharge. The paired active and passive views of the NSTX setup allows one, in principle, to account for nonstationary conditions. A number of conditions on the background emission are nonetheless required for a meaningful exploitation of this method. The most stringent condition relates to the toroidal uniformity of the features observed by the active and passive views. An analysis of the data from the active and passive views of the f-FIDA system indicates that, on average, a good correlation persists up to frequencies ≈ 10 kHz. This frequency range may extend up to 50 kHz (i.e., the usual upper limit for the f-FIDA system) for phenomena such as bursts of magnetohydrodynamic (MHD) activity, leading to an overall modest change in the macroscopic plasma parameters. The conditions are clearly violated for phenomena leading to a rapid change in the local plasma density and temperature, such as edge-localized modes, and to a macroscopic toroidal asymmetry, e.g., at the appearance of locked modes. At present, a rescaling of the active versus passive spectra is required, as no absolute intensity calibration is available. An intensity calibration, planned for the end of the run, will partly solve the ambiguity in the rescaling coefficients. However, the background levels of the paired views exhibit a different time evolution during a discharge. The most probable reason for that are the different paths inside the plasma and the different interception locations on the vacuum vessel walls. This effect cannot be removed *a priori* by an intensity calibration and must be accounted for by a software analysis for each discharge. In practice, the spectral region of 650.5–651 nm, where no fast-ion features are observed, is used to estimate the relative shift and rescale the active and passive spectra.

Data from a specific helium discharge are illustrated in Fig. 4. One NB source with beam voltage of 65 kV, corresponding to an injected power of 1 MW, is modulated at 330 Hz with 66% duty cycle. A clear modulation of the neutron rate is observed [Fig. 4(c)]. The net FIDA signal at $R=120$ cm is shown in Fig. 4(d). Two different approaches for background removal are compared: (i) exploitation of the spectral information from the background views and (ii) estimation of the background from the beam-off phases.

Data obtained by calculating the background from the passive views appear clearer. The FIDA signal is calculated by integrating the spectra over wavelengths corresponding to the 15–45 keV energy range of the measured photons. A

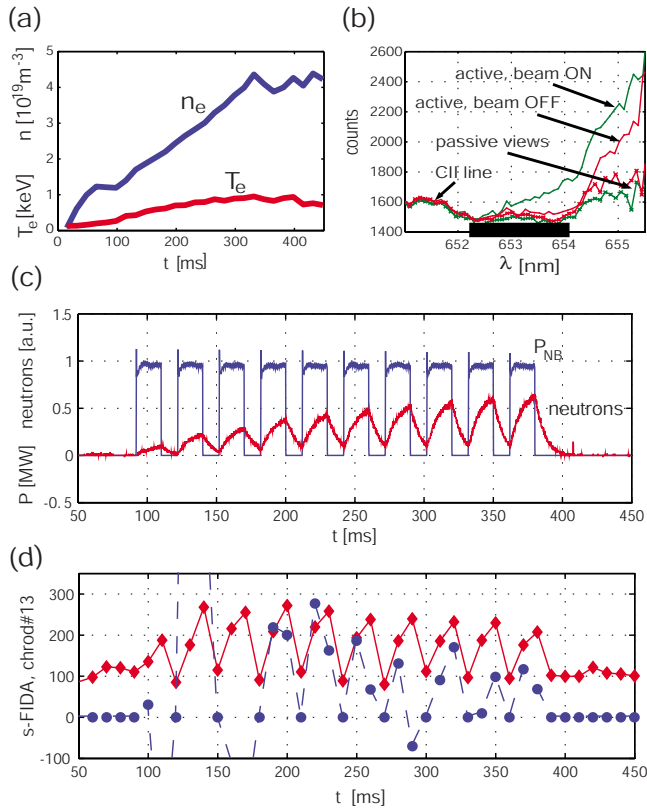


FIG. 4. (Color online) Comparison of background subtraction methods. (a) Density and electron temperature evolution for the target discharge. (b) Detail of the measured spectra at $R=120$ cm, including active/passive spectra during the NB on and off phases. The thick black line indicates the wavelength range over which spectra are integrated to obtain the net FIDA signal, [see Eq. (3)]. (c) NB power and neutron rate evolution. (d) Net FIDA signal at $R=120$ cm obtained with (diamonds, solid line) and without (circles, dashed line) the information from the passive view.

finite offset is observed, probably due to the different viewing geometries of the active and passive views. Examples of active and passive spectra at a specific time are shown in Fig. 4(b). A significant increase in the measured signal over the wavelength range of interest is observed for the beam-on phase. When the beam is turned off, the spectra collapse to the same level, except for the region close to the cold D_α line for $\lambda \gtrsim 654.5$ nm, where the contribution of halo neutrals may be significant. An impurity line, identified as C-II, is also visible at ≈ 651.5 nm. As it does not arise from charge exchange, its contribution is the same for active and passive views, and it does not contribute to the measured fast-ion signal. The consistency of the s-FIDA signals can be tested against the volume-integrated neutron rate, which is mainly determined by beam-plasma reactions. Although the s-FIDA temporal resolution does not allow an accurate estimate, the rise time during the beam-on phase is consistent with that observed in the neutron rate. However, the envelopes of the modulated FIDA and neutron signal differ. The continuous rise in the peak neutron rate as the discharge evolves does not reflect a similar behavior for the FIDA density. The nature of the two measurements, local versus volume averaged, may easily account for this discrepancy. A clear modulation of the signal is also obtained through the second method based on information from the active view only. However

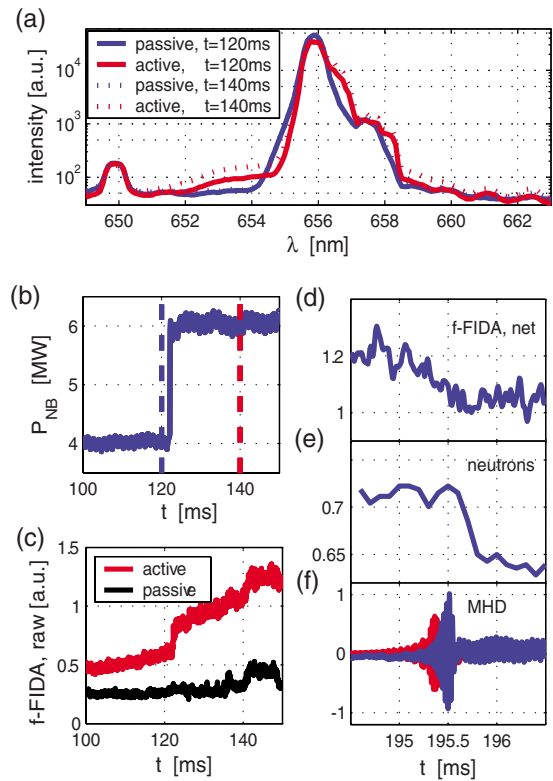


FIG. 5. (Color online) Signals from the FIDA systems. (a) Spectra from s-FIDA at $R=120$ cm before and after the third NB source is turned on. (b) Trace of the NB power. (c) Raw signals from f-FIDA at $R=120$ cm. (d) Net f-FIDA signal during a fast drop of the neutron rate [shown in (e)]. (f) Signals from magnetic probes measured at intermediate ($20 \leq f \leq 200$ kHz, red) and low ($f \leq 20$ kHz, blue) frequencies.

unphysical negative signals are observed, especially during the current ramp-up, for $t \leq 200$ ms. In conclusion, the information gathered through the background views improve the quality of the measurements. In order to fully exploit the paired-views concept, a more detailed investigation is needed to quantify the effects of the different viewing geometries and, possibly, of toroidal asymmetries on the measured signals. A FIDA simulation code,¹ recently adapted to the specific NSTX FIDA geometry, will help in assessing these issues, and the results will be the subject of future publications.

IV. EXAMPLES OF FIDA SIGNALS

Figure 5 shows further examples of FIDA signals from a deuterium plasma, with density $n_e \approx 3 \times 10^{19} \text{ m}^{-3}$ and electron temperature $T_e \approx 0.8$ keV. Three NBs are injected, with a beam voltage of 90 kV. The signals refer to times before and after the third source is switched on. Fast-ion signatures are expected to appear at the beam turn-on in the wavelength range of 650–655 nm and 657–662 nm, corresponding to the blueshifted and redshifted components, respectively. Spectra from a chord of the s-FIDA system looking at $R=120$ cm are illustrated in Fig. 5(a), and the evolution of the injected power is shown in Fig. 5(b). An enhancement of the counts is visible from the “bump” in the active spectrum in the region of 651–655 nm. No clear fast-ion features appear on the redshifted part of the spectrum. This region is con-

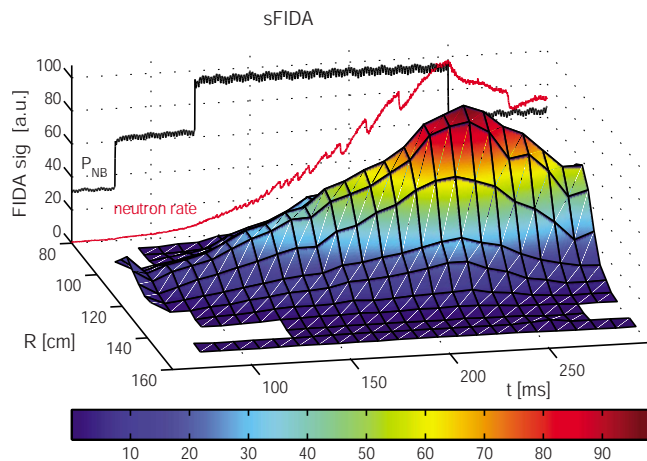


FIG. 6. (Color online) Example of a reconstructed temporal evolution of the FIDA density profile. The time traces of the injected NB power (black trace) and neutron rate (red trace) are also shown (in arbitrary units).

taminated by two strong C-II lines around 658 nm and by beam-neutral emission between 656 and 657 nm due to a finite projection of the sightline along the beam path. Another impurity line, identified as O-V, is present at 650 nm. Figure 5(c) shows the raw signals from the f-FIDA chords looking at $R=120$ cm. The onset of the third source is clearly seen as a prompt jump in the active signal due to the sudden increase in the injected neutrals. By comparing the net f-FIDA signal with the neutron rate, similarities appear during bursts of MHD activity, followed by a prompt drop in the neutron rate [Figs. 5(e) and 5(f)]. Consistently, a rapid varia-

tion in the f-FIDA signals is observed. As a final example, the reconstructed time evolution of the FIDA density radial profile is shown in Fig. 6.

ACKNOWLEDGMENTS

The support of PPPL and of the NSTX team is gratefully acknowledged. This work is supported by U.S. DOE Grant No. DE-FG02-06ER54867 and by U.S. DOE Contract No. DE-AC02-76CH03073.

- ¹Y. Luo, W. W. Heidbrink, K. H. Burrell, D. H. Kaplan, and P. Gohil, *Rev. Sci. Instrum.* **78**, 033505 (2007).
- ²W. W. Heidbrink, Y. Luo, K. H. Burrell, R. W. Harvey, R. I. Pinsker, and E. Ruskov, *Plasma Phys. Controlled Fusion* **49**, 1457 (2007).
- ³J. Egedal and H. Bindslev, *Phys. Plasmas* **11**, 2191 (2004).
- ⁴R. V. Budny, *Nucl. Fusion* **34**, 1247 (1994).
- ⁵E. D. Fredrickson, C. Z. Cheng, D. Darrow, G. Fu, N. N. Gorelenkov, G. Kramer, S. S. Medley, J. Menard, and A. L. Roquemore, *Phys. Plasmas* **10**, 2852 (2003).
- ⁶W. W. Heidbrink, K. H. Burrell, Y. Luo, N. A. Pablant, and E. Ruskov, *Plasma Phys. Controlled Fusion* **46**, 1855 (2004).
- ⁷K. Shinoara, D. S. Darrow, A. L. Roquemore, S. S. Medley, and F. E. Cecil, *Rev. Sci. Instrum.* **75**, 3640 (2004).
- ⁸S. S. Medley and A. L. Roquemore, *Rev. Sci. Instrum.* **75**, 3625 (2004).
- ⁹D. S. Darrow, *Rev. Sci. Instrum.* **79**, 023502 (2008).
- ¹⁰W. W. Heidbrink, R. E. Bell, Y. Luo, and W. Solomon, *Rev. Sci. Instrum.* **77**, 10F120 (2006).
- ¹¹R. E. Bell, *Rev. Sci. Instrum.* **75**, 4158 (2004).
- ¹²The bandpass filter comes from Barr Associates. The spectrometer is from Kaiser Optical Systems. The dispersion grating has a center wavelength of 656.1 nm and covers the range of 641.3–670.0 nm. The filter strips are obtained from a Kodak Wratten gelatine filter. The CCD camera is a PhotonMax 512B, Princeton Instruments/Acton. Both the chopper and chopper synchronizer unit are from Boston Electronics.
- ¹³The bandpass filter is from Chroma Technology. The photomultiplier is a Hamamatsu tube, model H8711-20. The acquisition system, from Vertilon Corporation, is a PhotoniQ IQSP480.